The Lennard-Jones equation of state revisited

By J. KARL JOHNSON, JOHN A. ZOLLWEG and KEITH E. GUBBINS

School of Chemical Engineering, Cornell University, Ithaca, NY 14853, USA

We review the existing simulation data and equations of state for the Lennard-Jones (LJ) fluid, and present new simulation results for both the cut and shifted and the full LJ potential. New parameters for the modified Benedict–Webb–Rubin (MBWR) equation of state used by Nicolas, Gubbins, Streett and Tildesley are presented. In contrast to previous equations, the new equation is accurate for calculations of vapour–liquid equilibria. The equation also accurately correlates pressures and internal energies from the triple point to about 4·5 times the critical temperature over the entire fluid range. An equation of state for the cut and shifted LJ fluid is presented and compared with the simulation data of this work, and previously published Gibbs ensemble data. The MBWR equation of state can be extended to mixtures via the van der Waals one-fluid theory mixing rules. Calculations for binary fluid mixtures are found to be accurate when compared with Gibbs ensemble simulations.

1. Introduction

The Lennard-Jones 12-6 (LJ) potential is an important model for exploring the behaviour of simple fluids, and has been used to study vapour–liquid and liquid-liquid equilibria, melting, behaviour of fluids confined within small pores, small atomic clusters, a variety of surface and transport properties, and so on. It has also been widely used as a reference fluid in perturbation treatments for more complex fluids. In many ways, the LJ model is oversimplified [1]; for example, the form of the repulsive part of the potential is incorrect, being insufficiently repulsive at short distances, the C_6 dispersion coefficient is too high while higher dispersion coefficients are neglected, and its application to dense systems neglects three-body forces completely. Nevertheless, it captures much of the essential physics of simple fluids.

There have been a number of attempts to fit simulation data for the LJ fluid to an analytical equation of state [2–12]. One of the most successful of these is the equation of state of Nicolas et al. [5]. The Nicolas et al. equation of state uses a modified Benedict–Webb–Rubin (MBWR) equation having 33 parameters, 32 of which are linear. This large number of adjustable parameters gives the equation sufficient flexibility to correlate data accurately over a wide range of state conditions.

The parameters for the Nicolas EOS were regressed from simulation data generated by Nicolas et al. and by previous workers [2–5, 13–17], mainly from the late 1960s and early 1970s. By current standards, these data were, for the most part, for small systems and short run times. In addition, there were few vapour–liquid equilibrium (VLE) data available, and the critical point of the LJ fluid was not known accurately. Nicolas et al. chose to constrain their equation of state to give critical density and temperature values of $\rho_c^* = 0.35$, and $T_c^* = 1.35$, where $\rho^* = (N/V)\sigma^3$,

N is the number of atoms, V is the volume of the system, σ is the LJ diameter, and $T^* = kT/\epsilon$ where k is Boltzmann's constant, T is the temperature in Kelvins, and ϵ is the LJ potential well depth. These values lay within the older estimates of the critical properties given by Verlet [13]. Recent simulations show that $T_c^* = 1 \cdot 35$ is too high.

In recent years, the Gibbs ensemble Monte Carlo technique of Panagiotopoulos [18, 19] has proved particularly suitable for the direct determination of coexistence properties and for estimating critical points [20, 21]. Simulations in the Gibbs ensemble by several workers [18–20, 22, 23] have provided many more coexistence data for the LJ fluid, along with more reliable estimates for the critical temperature and density. The best current estimate of the critical point for the full LJ fluid predicted from Gibbs ensemble simulations is $\rho_c^* = 0 \cdot 304 \pm 0 \cdot 006$ and $T_c^* = 1 \cdot 316 \pm 0 \cdot 006$ [20, 21]. Lotfi *et al.* [11] have recently completed a study of the vapour–liquid coexistence properties of the pure LJ fluid by using isothermal–isobaric (NPT) ensemble simulations in conjunction with Widom's particle insertion method. Their data provide additional estimates of the critical properties as well as independent saturation densities and pressures. The data of Lotfi *et al.* are generally in very good agreement with the previous Gibbs ensemble results.

The Nicolas *et al.* equation of state does not accurately predict the saturation properties when compared with the recent Gibbs ensemble and Lotfi *et al.* data. Such discrepancies are particularly troublesome when using an equation of state for the LJ fluid as a reference term in perturbation theories of molecular fluids.

In this paper, we present new simulation data for the LJ fluid (section 2.2). These new data are used to refit the parameters in the MBWR equation (section 4). We do not use any VLE data in the fit, but we do constrain the parameters to give a critical density and temperature that agree with values estimated from the Gibbs ensemble and Lotfi *et al.* simulations. We demonstrate that the new parameters for the MBWR equation correlate accurately the simulation data, and that saturation vapour pressures and densities are predicted accurately when compared with recent simulation results.

2. Simulation data for the Lennard-Jones fluid

The full LJ potential is given by

$$\phi(r) = 4\epsilon \left[\left(\frac{\sigma}{r} \right)^{12} - \left(\frac{\sigma}{r} \right)^6 \right], \tag{1}$$

where ϵ is the LJ well depth and σ is the LJ atomic diameter. In computer simulations the potential must be truncated at some point $r_c \leq L/2$, where r_c is the cutoff of the potential and L is the simulation box length. In practice, three types of truncated potential have been used: (1) cut potential (not shifted), (2) cut and shifted potential, and (3) cut and shifted force potential [24]. The cut and shifted force potential has the advantage in molecular dynamics (MD) simulations that there is no discontinuity in the potential or the force [5]. Corrections must be applied to the simulation results for each of these potentials in order to approximate the properties of the full LJ fluid. In each case, long range or tail corrections are computed by assuming that the pair correlation function is unity ($g(r) = 1$) for $r > r_c$. This leads to the following

Table 1. Summary of published thermodynamic data for the LJ fluid. Run length for MD is in time steps, for MC run length is in configurations. For simulations in the NVE ensemble the temperature range was covered sporadically.

Source	Method	Run length		N	r_c/σ	Range	
		Equil.	Prod.			T^*	ρ^*
Wood and Parker, 1957 [25, 26]	MC	—	$\sim 10^5$	32, 108	0.9–3.8	1.06–100	0.05–3
Verlet, 1967 [13]	NVE MD	300	1200	864	2.5	0.591–4.625	0.35–0.88
Levesque and Verlet, 1969 [2]	MC	—	4×10^4	864	2.5	1.35, 2.74	0.3–0.95
Levesque and Verlet, 1969 [2]	NVE MD	300	1200	864	2.5	0.76–3.67	0.35–0.85
Hansen and Verlet, 1969 [14]	MC	—	$\sim 10^6$	864	2.5	0.75, 1.15	0.02–0.92
Hansen, 1970 [3]	MC	10^5	5×10^5	864	—	2.74–100	0.4–1.77
McDonald and Singer, 1972 [4]	MC	—	5×10^4	108, 256	~ 2.5	0.551–1.237	0.65–0.96
Adams, 1975 [16]	GCMC	—	10^6	20–200	—	2.0, 4.0	0.02–0.85
Adams, 1976 [17]	GCMC	—	10^6	~ 200	—	1.0–1.2	0.62–0.82
Adams, 1979 [27]	GCMC	—	$10^6 - 6 \times 10^6$	~ 6000	2.62	1.15–1.35	0.04–0.675
Nicolas et al., 1979 [5]	NVE MD	$2\sigma^a$	5000	256	2.5	0.48–6.01	0.35–1.2
Nakanishi, 1986 [28]	NVE MD	10^4	5000	108, 256	—	0.71	0.5–1.5
Adachi et al., 1988 [8]	NVE MD	500	3500	108, 256	—	0.7–2.94	0.05–1.1
Shaw, 1988 [29]	Density of states MC			122	$L/2^b$	1.157–6.197	0.6–1.2
Saager and Fischer, 1990 [30]	NVT MD	6×10^4	1.5×10^5	256	$L/2^b$	0.567–4.002	0.215–1.1
Lotfi et al., 1992 [11]	NPT MD	5000	55000	1372	$L/2^b$	0.7–1.3	0.06–0.84
Miyano, 1992 [12]	MC	10^6	1.5×10^6	256	$L/2^b$	0.45–100	0.2–1.1
This work	NVT MD	$3\sigma^a$	2×10^4	864	4.0	0.7–6.0	0.005–1.25
This work	MC	2.5×10^6	1.5×10^7	500	≥ 4.0	1.0–5.0	0.05–0.9

[a] Equilibration was carried out for the specified root mean square displacement.
[b] Cutoff was set to half the box length.

tail corrections for the pressure P_{lrc}^* and internal energy U_{lrc}^* [24],

$$P_{lrc}^* = \frac{32}{9} \pi \rho^{*2} \left[\left(\frac{\sigma}{r_c} \right)^9 - 3/2 \left(\frac{\sigma}{r_c} \right)^3 \right], \qquad (2)$$

$$U_{lrc}^* = \frac{8}{9} \pi \rho^* \left[\left(\frac{\sigma}{r_c} \right)^9 - 3 \left(\frac{\sigma}{r_c} \right)^3 \right]. \qquad (3)$$

In the vast majority of cases the LJ data published in the literature have made use of these long range corrections.

2.1. *Literature data*

Wood and Parker [25] at Los Alamos National Laboratory were the first to publish properties of the 3-dimensional LJ fluid from computer simulations. Since that time, many other authors have also performed simulations on the LJ fluid and published their findings. In table 1 we summarize the simulation results for much of the work on the thermodynamic properties of the LJ fluid. These include the following works: Wood and Parker, 1957 [25]; Verlet, 1967 [13]; Wood, 1968 [26]; Levesque and Verlet, 1969 [2]; Hansen and Verlet, 1969 [14]; Hansen, 1970 [3]; McDonald and Singer, 1972 [4]; Adams, 1975, 1976, and 1979 [16, 17, 27]; Nicolas *et al.*, 1979 [5]; Nakanishi, 1986 [28]; Adachi *et al.*, 1988 [8]; Shaw, 1988 [29]; Saager and Fisher, 1990 [30]; Lotfi *et al.*, 1992 [11]; and Miyano, 1992 [12]. We note that Verlet and Weis [15] reported in 1972 previously published simulation results of [2, 3, 14], and augmented these data with either internal energy values or additional data points that were not reported in the original sources.

2.2. *Simulation data from this work*

We have performed simulations of the LJ fluid using both the MD and MC techniques. The bulk of the data are from MD simulations and are presented in table 2. For these simulations we used the cut and shifted potential $\phi_{cs}(r)$ given by

$$\phi_{cs}(r) = \begin{cases} \phi(r) - \phi(r_c) & \text{if } r < r_c \\ 0 & \text{if } r > r_c. \end{cases} \qquad (4)$$

We used a system size of 864 atoms and a cutoff of $r_c = 4 \cdot 0\sigma$. Because of the large cutoff we expect any effect due to the discontinuity of the force at r_c to be negligible. The full potential energies and pressures were recovered by adding back the potential shift and applying the standard long range corrections given by equations (2) and (3). Vogelsang and Hoheisel [31] have used Baxter's continuation method to study the effect of the cutoff on thermodynamic properties. They found that for $r_c \geq 4 \cdot 3\sigma$ the normal long range corrections are practically exact for conditions close to the triple point. At higher temperatures or lower densities the effect of the cutoff is expected to be even smaller. We have compared our simulation results with data from very accurate simulations of Thompson [32] for a system of 1372 LJ atoms with the same cutoff. These independent data serve as a check of our coding and simulation technique. We found the agreement to be excellent. The temperature range covered in the simulations was $0 \cdot 7 \leq T^* \leq 6 \cdot 0$. This covers a range from about the triple point ($T_{tp}^* \approx 0 \cdot 69$) to four and a half times the critical temperature ($T_c^* \approx 1 \cdot 31$). The densities ranged from $0 \cdot 1 \leq \rho^* \leq 1 \cdot 25$ at the highest temperature,

Table 2. Molecular dynamics simulation results of this work. The numbers in parentheses are the estimated errors of the mean in the last decimal place, e.g., $8 \cdot 51(2) = 8 \cdot 51 \pm 0 \cdot 02$.

ρ^*	T^*	P^*	U^*	P_{cs}^*	U_{cs}^*	Steps	δt^*
0·1	6·0	0·6499(6)	−0·478(2)	0·6525	−0·452	30 000	0·002
0·2	6·0	1·442(1)	−0·942(2)	1·452	−0·890	30 000	0·002
0·3	6·0	2·465(3)	−1·376(1)	2·489	−1·298	30 000	0·002
0·4	6·0	3·838(5)	−1·785(3)	3·880	−1·681	20 000	0·002
0·5	6·0	5·77(1)	−2·131(3)	5·84	−2·000	20 000	0·002
0·6	6·0	8·51(2)	−2·382(5)	8·60	−2·225	20 000	0·002
0·7	6·0	12·43(2)	−2·501(4)	12·56	−2·318	20 000	0·002
0·8	6·0	18·05(2)	−2·416(4)	18·22	−2·207	20 000	0·002
0·9	6·0	26·00(2)	−2·058(4)	26·21	−1·823	20 000	0·004
1·0	6·0	37·06(3)	−1·361(6)	37·32	−1·100	20 000	0·002
1·1	6·0	52·25(2)	−0·216(4)	52·57	0·072	20 000	0·002
1·2	6·0	72·90(5)	1·502(9)	73·28	1·816	20 000	0·002
1·25	6·0	85·71(5)	2·612(8)	86·12	2·939	20 000	0·002
0·1	5·0	0·5324(4)	−0·510(2)	0·5350	−0·484	30 000	0·002
0·2	5·0	1·166(2)	−1·012(2)	1·176	−0·960	30 000	0·002
0·3	5·0	1·974(3)	−1·500(2)	1·998	−1·422	30 000	0·002
0·4	5·0	3·087(7)	−1·955(2)	3·129	−1·851	30 000	0·002
0·5	5·0	4·668(8)	−2·360(2)	4·733	−2·230	30 000	0·002
0·6	5·0	6·97(1)	−2·688(4)	7·06	−2·531	20 000	0·002
0·7	5·0	10·30(2)	−2·902(5)	10·43	−2·719	20 000	0·002
0·8	5·0	15·14(2)	−2·948(4)	15·31	−2·739	20 000	0·002
0·9	5·0	22·22(2)	−2·720(5)	22·43	−2·485	20 000	0·002
1·0	5·0	32·23(3)	−2·168(6)	32·49	−1·907	20 000	0·002
1·1	5·0	46·28(4)	−1·165(7)	46·60	−0·877	20 000	0·002
1·2	5·0	65·46(5)	0·370(8)	65·84	0·684	20 000	0·002
0·1	4·0	0·4154(6)	−0·547(1)	0·4180	−0·521	30 000	0·002
0·2	4·0	0·894(2)	−1·088(2)	0·9045	−1·036	30 000	0·002
0·3	4·0	1·501(3)	−1·614(2)	1·525	−1·536	30 000	0·002
0·4	4·0	2·319(4)	−2·125(3)	2·361	−2·021	20 000	0·002
0·5	4·0	3·532(6)	−2·605(3)	3·597	−2·475	20 000	0·002
0·6	4·0	5·33(1)	−3·017(4)	5·42	−2·860	20 000	0·002
0·7	4·0	8·044(1)	−3·335(4)	8·172	−3·152	20 000	0·002
0·8	4·0	12·14(2)	−3·494(5)	12·31	−3·285	20 000	0·002
0·9	4·0	18·24(1)	−3·415(3)	18·45	−3·180	20 000	0·002
1·0	4·0	27·11(2)	−3·023(4)	27·37	−2·762	20 000	0·002
1·1	4·0	39·74(4)	−2·217(8)	40·05	−1·929	20 000	0·002
1·2	4·0	57·41(2)	−0·866(3)	57·79	−0·552	20 000	0·002
0·1	3·0	0·2984(1)	−0·592(2)	0·3010	−0·566	30 000	0·003
0·2	3·0	0·615(1)	−1·178(2)	0·625	−1·126	30 000	0·003
0·3	3·0	0·999(2)	−1·751(2)	1·023	−1·673	30 000	0·003
0·4	3·0	1·529(5)	−2·314(2)	1·571	−2·210	20 000	0·003
0·5	3·0	2·336(8)	−2·860(2)	2·401	−2·729	20 000	0·003
0·6	3·0	3·60(1)	−3·369(3)	3·69	−3·212	20 000	0·003
0·7	3·0	5·65(1)	−3·795(2)	5·78	−3·612	20 000	0·003
0·8	3·0	8·92(1)	−4·083(3)	9·09	−3·874	20 000	0·003
0·9	3·0	13·95(1)	−4·170(3)	14·16	−3·935	20 000	0·003
1·0	3·0	21·52(2)	−3·967(3)	21·78	−3·705	20 000	0·002
1·1	3·0	32·64(2)	−3·365(4)	32·96	−3·077	20 000	0·002

Table 2. Continued

ρ^*	T^*	P^*	U^*	P_{cs}^*	U_{cs}^*	Steps	δt^*
0·1	2·5	0·2383(3)	−0·625(2)	0·2409	−0·599	30 000	0·003
0·2	2·5	0·472(1)	−1·234(3)	0·482	−1·182	30 000	0·003
0·3	2·5	0·746(2)	−1·826(2)	0·770	−1·748	30 000	0·003
0·4	2·5	1·123(2)	−2·419(2)	1·165	−2·315	40 000	0·003
0·5	2·5	1·706(4)	−3·002(2)	1·771	−2·871	20 000	0·003
0·6	2·5	2·71(1)	−3·553(2)	2·80	−3·396	20 000	0·003
0·7	2·5	4·365(7)	−4·043(2)	4·493	−3·860	20 000	0·003
0·8	2·5	7·17(1)	−4·404(2)	7·34	−4·195	20 000	0·003
0·9	2·5	11·61(1)	−4·583(3)	11·82	−4·348	20 000	0·003
1·0	2·5	18·47(2)	−4·484(4)	18·73	−4·222	20 000	0·002
1·05	2·5	23·18(1)	−4·284(2)	23·47	−4·009	20 000	0·003
0·1	2·0	0·1776(2)	−0·669(2)	0·1802	−0·643	30 000	0·003
0·2	2·0	0·329(1)	−1·308(3)	0·339	−1·256	30 000	0·003
0·3	2·0	0·489(2)	−1·922(3)	0·513	−1·844	30 000	0·003
0·4	2·0	0·700(3)	−2·539(3)	0·742	−2·435	20 000	0·003
0·5	2·0	1·071(4)	−3·149(2)	1·136	−3·018	20 000	0·003
0·6	2·0	1·75(1)	−3·747(2)	1·84	−3·590	20 000	0·003
0·7	2·0	3·028(7)	−4·300(1)	3·156	−4·117	20 000	0·003
0·8	2·0	5·285(7)	−4·752(1)	5·453	−4·543	20 000	0·003
0·9	2·0	9·12(1)	−5·025(2)	9·33	−4·790	20 000	0·003
1·0	2·0	15·20(2)	−5·040(4)	15·46	−4·778	20 000	0·003
1·05	2·0	19·46(2)	−4·904(4)	19·75	−4·629	20 000	0·003
0·1	1·8	0·1533(2)	−0·689(2)	0·1559	−0·663	50 000	0·004
0·1	1·8	0·1538(2)	−0·683(2)	0·1564	−0·657	30 000	0·004
0·2	1·8	0·2704(8)	−1·352(3)	0·2808	−1·299	30 000	0·004
0·3	1·8	0·384(1)	−1·973(2)	0·4076	−1·894	30 000	0·004
0·4	1·8	0·538(2)	−2·592(3)	0·580	−2·487	20 000	0·004
0·5	1·8	0·818(4)	−3·210(2)	0·883	−3·079	20 000	0·004
0·6	1·8	1·364(7)	−3·831(2)	1·458	−3·674	20 000	0·004
0·7	1·8	2·46(1)	−4·410(2)	2·59	−4·227	20 000	0·004
0·8	1·8	4·51(1)	−4·895(2)	4·68	−4·686	20 000	0·004
0·9	1·8	8·06(1)	−5·211(2)	8·27	−4·976	20 000	0·004
1·0	1·8	13·83(2)	−5·272(3)	14·09	−5·010	20 000	0·004
0·1	1·6	0·1288(3)	−0·717(3)	0·1314	−0·691	30 000	0·004
0·2	1·6	0·2119(7)	−1·401(5)	0·2223	−1·348	30 000	0·004
0·3	1·6	0·277(1)	−2·030(6)	0·301	−1·951	30 000	0·003
0·4	1·6	0·363(3)	−2·661(4)	0·405	−2·556	20 000	0·004
0·5	1·6	0·552(3)	−3·284(2)	0·617	−3·153	20 000	0·004
0·6	1·6	0·967(4)	−3·916(1)	1·061	−3·759	20 000	0·004
0·7	1·6	1·889(7)	−4·519(1)	2·017	−4·336	20 000	0·004
0·8	1·6	3·69(1)	−5·045(2)	3·86	−4·836	20 000	0·004
0·9	1·6	6·957(7)	−5·406(1)	7·169	−5·171	20 000	0·004
1·0	1·6	12·39(1)	−5·517(2)	12·65	−5·255	20 000	0·004

Table 2. Continued

ρ^*	T^*	P^*	U^*	P_{cs}^*	U_{cs}^*	Steps	δt^*
0·1	1·4	0·1035(3)	−0·766(3)	0·1061	−0·740	30 000	0·004
0·2	1·4	0·1524(4)	−1·483(4)	0·1628	−1·430	30 000	0·004
0·3	1·4	0·172(1)	−2·136(6)	0·196	−2·057	20 000	0·004
0·4	1·4	0·196(2)	−2·74(5)	0·238	−2·64	20 000	0·004
0·5	1·4	0·281(5)	−3·366(3)	0·346	−3·235	20 000	0·004
0·6	1·4	0·565(2)	−4·006(1)	0·659	−3·849	20 000	0·004
0·7	1·4	1·292(5)	−4·637(1)	1·420	−4·454	20 000	0·004
0·8	1·4	2·856(8)	−5·199(2)	3·024	−4·990	20 000	0·004
0·9	1·4	5·795(8)	−5·612(2)	6·007	−5·377	20 000	0·004
1·0	1·4	10·86(1)	−5·778(3)	11·12	−5·516	20 000	0·004
0·1	1·3	0·0909(2)	−0·795(4)	0·0935	−0·768	30 000	0·004
0·2	1·3	0·1216(6)	−1·544(4)	0·1321	−1·491	30 000	0·004
0·4	1·3	0·115(2)	−2·803(7)	0·157	−2·698	20 000	0·004
0·5	1·3	0·152(3)	−3·412(3)	0·217	−3·281	20 000	0·004
0·6	1·3	0·358(4)	−4·056(2)	0·452	−3·899	20 000	0·004
0·7	1·3	0·981(9)	−4·697(1)	1·109	−4·514	20 000	0·004
0·8	1·3	2·412(7)	−5·279(1)	2·580	−5·070	20 000	0·004
0·9	1·3	5·21(1)	−5·714(2)	5·42	−5·479	20 000	0·004
0·95	1·3	7·32(1)	−5·851(3)	7·56	−5·602	20 000	0·004
0·05	1·2	0·048 87(6)	−0·421(2)	0·049 52	−0·408	40 000	0·004
0·1	1·2	0·0770(4)	−0·854(8)	0·0796	−0·827	30 000	0·004
0·5	1·2	0·017(5)	−3·466(7)	0·082	−3·335	20 000	0·004
0·6	1·2	0·148(3)	−4·103(1)	0·242	−3·946	20 000	0·004
0·7	1·2	0·673(6)	−4·757(1)	0·801	−4·574	20 000	0·004
0·8	1·2	1·967(6)	−5·362(1)	2·135	−5·153	20 000	0·004
0·9	1·2	4·57(1)	−5·827(2)	4·78	−5·592	20 000	0·004
0·95	1·2	6·62(1)	−5·973(2)	6·86	−5·724	20 000	0·004
0·05	1·15	0·045 75(6)	−0·438(3)	0·0464	−0·425	40 000	0·004
0·1	1·15	0·0704(3)	−0·863(7)	0·0730	−0·836	40 000	0·004
0·55	1·15	−0·031(3)	−3·806(2)	0·048	−3·662	20 000	0·004
0·6	1·15	0·043(7)	−4·129(2)	0·137	−3·972	40 000	0·004
0·7	1·15	0·498(5)	−4·790(1)	0·626	−4·607	20 000	0·004
0·8	1·15	1·739(7)	−5·403(1)	1·907	−5·194	20 000	0·004
0·9	1·15	4·26(1)	−5·882(2)	4·47	−5·647	20 000	0·004
0·95	1·15	6·24(1)	−6·040(2)	6·48	−5·791	20 000	0·004
0·05	1·1	0·0431(1)	−0·444(2)	0·0438	−0·431	40 000	0·004
0·55	1·1	−0·106(3)	−3·844(3)	−0·027	−3·700	30 000	0·004
0·6	1.1	−0·068(4)	−4·156(2)	0·026	−3·999	20 000	0·004
0·7	1.1	0·346(4)	−4·824(1)	0·474	−4·641	20 000	0·004
0·8	1.1	1·495(9)	−5·448(2)	1·663	−5·239	20 000	0·004
0·9	1.1	3·92(1)	−5·941(2)	4·13	−5·706	20 000	0·004
0·95	1.1	5·889(7)	−6·099(1)	6·125	−5·850	20 000	0·004
0·05	1·05	0·0401(1)	−0·460(3)	0·0408	−0·447	40 000	0·004
0·6	1·05	−0·172(5)	−4·189(3)	−0·078	−4·032	20 000	0·004
0·7	1·05	0·179(4)	−4·858(1)	0·307	−4·675	20 000	0·004
0·8	1·05	1·259(8)	−5·490(2)	1·427	−5·281	20 000	0·004
0·9	1·05	3·597(9)	−5·999(2)	3·809	−5·764	20 000	0·004
0·95	1·05	5·47(1)	−6·172(2)	5·71	−5·923	20 000	0·004

J. K. Johnson *et al.*

Table 2. Continued

ρ^*	T^*	P^*	U^*	P_{cs}^*	U_{cs}^*	Steps	δt^*
0·05	1·0	0·0368(1)	−0·483(5)	0·0375	−0·469	40 000	0·004
0·6	1·0	−0·272(5)	−4·223(3)	−0·178	−4·066	20 000	0·004
0·7	1·0	0·015(5)	−4·887(1)	0·143	−4·704	20 000	0·004
0·8	1·0	1·011(6)	−5·535(1)	1·179	−5·326	20 000	0·004
0·9	1·0	3·28(1)	−6·055(2)	3·49	−5·819	20 000	0·004
0·95	1·0	5·131(8)	−6·231(2)	5·367	−5·982	20 000	0·004
0·01	0·95	0·008 95(1)	−0·096(2)	0·008 98	−0·093	40 000	0·004
0·05	0·95	0·0339(1)	−0·504(7)	0·0346	−0·490	40 000	0·004
0·6	0·95	−0·371(6)	−4·262(5)	−0·277	−4·105	20 000	0·004
0·7	0·95	−0·149(3)	−4·921(1)	−0·021	−4·738	20 000	0·004
0·8	0·95	0·770(7)	−5·579(1)	0·938	−5·370	20 000	0·004
0·9	0·95	2·93(1)	−6·117(2)	3·14	−5·882	20 000	0·004
0·95	0·95	4·712(8)	−6·302(1)	4·948	−6·053	20 000	0·004
0·005	0·9	0·004 36(3)	−0·051(2)	0·004 37	−0·050	40 000	0·004
0·01	0·9	0·008 42(1)	−0·102(1)	0·008 45	−0·099	40 000	0·004
0·65	0·9	−0·461(6)	−4·616(2)	−0·350	−4·446	20 000	0·004
0·7	0·9	−0·317(5)	−4·962(2)	−0·189	−4·779	20 000	0·004
0·8	0·9	0·534(7)	−5·623(1)	0·702	−5·414	20 000	0·004
0·9	0·9	2·583(9)	−6·176(2)	2·795	−5·941	20 000	0·004
0·005	0·85	0·004 11(1)	−0·048(1)	0·004 12	−0·047	150 000	0·006
0·005	0·85	0·004 09(4)	−0·0559(7)	0·004 10	−0·0546	40 000	0·004
0·01	0·85	0·007 91(1)	−0·104(1)	0·007 94	−0·101	40 000	0·004
0·7	0·85	−0·487(3)	−4·995(1)	−0·359	−4·812	20 000	0·004
0·8	0·85	0·273(7)	−5·670(1)	0·441	−5·461	20 000	0·004
0·9	0·85	2·24(1)	−6·236(2)	2·45	−6·000	20 000	0·004
0·005	0·8	0·003 84(1)	−0·054(1)	0·003 85	−0·053	150 000	0·006
0·005	0·8	0·003 84(4)	−0·056(1)	0·003 85	−0·055	40 000	0·004
0·01	0·8	0·007 36(1)	−0·114(2)	0·007 39	−0·111	40 000	0·004
0·7	0·8	−0·649(5)	−5·034(2)	−0·521	−4·851	20 000	0·004
0·8	0·8	0·014(7)	−5·717(1)	0·182	−5·508	20 000	0·004
0·9	0·8	1·87(1)	−6·302(2)	2·08	−6·066	20 000	0·004
0·9	0·8	1·87(1)	−6·301(2)	2·08	−6·065	20 000	0·004
0·005	0·75	0·003 59(1)	−0·0554(7)	0·003 60	−0·0540	150 000	0·006
0·005	0·75	0·003 58(5)	−0·0613(8)	0·003 59	−0·0599	40 000	0·004
0·01	0·75	0·006 84(1)	−0·115(2)	0·006 87	−0·112	100 000	0·006
0·01	0·75	0·006 85(1)	−0·113(1)	0·006 88	−0·110	40 000	0·004
0·7	0·75	−0·834(7)	−5·070(2)	−0·706	−4·887	20 000	0·004
0·8	0·75	−0·256(5)	−5·765(1)	−0·088	−5·556	20 000	0·004
0·9	0·75	1·503(9)	−6·365(2)	1·715	−6·129	20 000	0·004
0·005	0·7	0·003 33(1)	−0·0596(6)	0·003 33	−0·0606	40 000	0·004
0·005	0·7	0·003 32(1)	−0·062(1)	0·003 34	−0·058	150 000	0·006
0·8	0·7	−0·525(7)	−5·815(1)	−0·357	−5·606	20 000	0·004
0·9	0·7	1·14(1)	−6·429(2)	1·35	−6·193	20 000	0·004

$T^* = 6\cdot0$, to $0\cdot005 \leq \rho^* \leq 0\cdot9$ at the lowest temperature, $T^* = 0\cdot7$. Liquid-like state points were equilibrated until the root-mean-square (r.m.s.) displacement for the system reached 3σ or more. For the low density points, equilibration was carried out for 5 000 to 20 000 time steps, rather than for a given r.m.s. displacement. Averages were collected from runs of 2×10^4 time steps for the liquid-like densities and runs of 4×10^4 time steps for low density state points. At the lowest density ($\rho^* = 0\cdot005$) we repeated some runs, taking data for $1\cdot5 \times 10^5$ time steps. The sample variances of the mean for pressure and internal energy were calculated by dividing the data-taking run into ten sub-blocks. The computed means from each of these sub-blocks were used to calculate the sample variance of the mean as described by Bishop and Frinks [33]. We also report in table 2 the pressures P_{cs}^* and internal energies U_{cs}^* for the fluid interacting through the cut and shifted potential, equation (4). The estimated errors are approximately the same as values reported for P^* and U^* in table 2.

Our data set includes some points in the metastable regions for both the vapour–liquid and liquid–solid phase transitions. We have, however, been careful not to sample regions past the spinodal curve when we knew its approximate location *a priori*. We fitted the pressure and internal energy data to two different rational polynomials in order to identify any points that did not fit smoothly with the rest of the data. Using this criterion we excluded several data points that appeared to be in the unstable vapour–liquid region. These points are not included in table 2, nor were they included in the fitting procedure of section 4.1.

We used the velocity Verlet [34] algorithm for integrating the equations of motion, and simple momentum scaling at every time step to sample the NVT ensemble. When using molecular dynamics it is important to choose a time step δt small enough to solve the equations of motion accurately, but large enough to sample phase space adequately. Because our calculations covered such a wide range of densities and temperatures we did not use the same time step at every state point. We have performed short NVE ensemble simulations at various temperatures and densities in order to choose a $\delta t^* = (\delta t/\sigma)(\epsilon/m)^{1/2}$ that gives good total energy conservation, i.e., fluctuations in total energy, $\langle \delta \mathscr{H}^2 \rangle^{1/2}$, on the order of 10^{-4}, where $\mathscr{H}$ is the Hamiltonian of the system. The actual time step used for each run is listed in table 2.
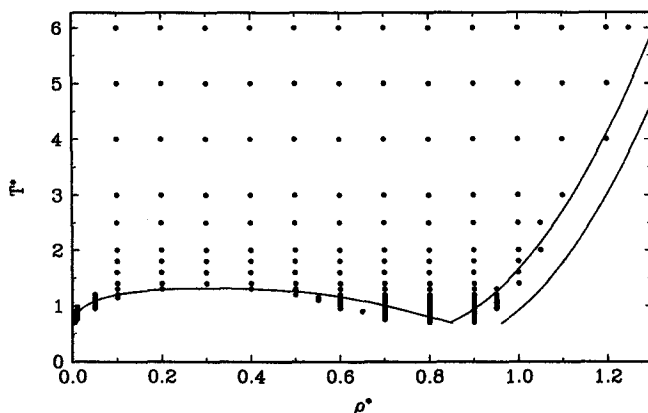
Figure 1. The T^*–ρ^* projection of the MD simulation points reported in this work. The parameters in the equation were regressed from these data.

We plot the temperature–density range covered by our MD simulations in figure 1. We have also plotted the vapour–liquid phase envelope and the solid–liquid coexistence curves. The vapour–liquid curve is from calculations made with the new MBWR parameters of this work. The solid–liquid curves were sketched from the simulation data of Chokappa and Clancy [35] and Hansen and Verlet [14]. The best estimate for the triple point temperature from these references is $T_{tp}^* \approx 0.69$.

Results of our MC simulations are presented in table 3. We used the cut potential on a system of 500 atoms and conventional NVT MC. The cutoff varied, but in all cases $r_c \geq 4.0\sigma$, with the specific cutoff listed in table 3. The standard long range corrections given by equations (2) and (3) were applied. We typically equilibrated the system for 2.5×10^6 configurations, followed by averaging for approximately 1.5×10^7 configurations. The maximum displacement step size was adjusted during equilibration to achieve an acceptance ratio of about 40%. We also collected $g(r)$ data from both the MD and MC simulations for other purposes. The MC data provide an independent route to thermodynamic properties of the LJ fluid, and thus serve as an additional check of our coding. The MD and MC simulation results generally agree to within one standard deviation; a few points lie within two standard deviations.

3. Equations of state for the Lennard-Jones fluid

Equations of state for the LJ fluid can be divided roughly into two groups: (1) equations having some theoretical basis (semitheoretical), and (2) purely empirical equations of state. This distinction can become blurred at times because semi-theoretical equations can contain a large number of adjustable parameters, making them much like empirical equations. In this section we review briefly the available equations of state for the LJ fluid. We present a summary of the published equations of state in table 4.

Several equations of state have been published that are based on perturbation

Table 3.   Monte Carlo simulation results of this work.

$\rho*$	T^*	P^*	U^*	r_c/σ
0·5	5·0	4·654(3)	−2·365(1)	4·0
0·1	2·0	0·1777(2)	−0·667(1)	5·0
0·2	2·0	0·3290(6)	−1·306(1)	5·0
0·4	2·0	0·705(1)	−2·538(2)	5·0
0·5	2·0	1·069(3)	−3·149(2)	5·0
0·6	2·0	1·756(7)	−3·746(2)	4·71
0·7	2·0	3·024(7)	−4·300(2)	4·47
0·8	2·0	5·28(1)	−4·753(3)	4·27
0·9	2·0	9·09(2)	−5·030(4)	4·11
0·1	1·2	0·0776(1)	−0·840(2)	4·0
0·1	1·15	0·0707(1)	−0·869(1)	4·0
0·05	1·0	0·0369(1)	−0·478(1)	5·0
0·6	1·0	−0·269(9)	−4·228(6)	4·71
0·7	1·0	0·019(10)	−4·890(2)	4·47
0·8	1·0	1·03(1)	−5·533(1)	4·27
0·8	1·0	1·009(3)	−5·5357(6)	4·0
0·9	1·0	3·24(2)	−6·062(4)	4·11

Table 4. Summary of published equations of state for the LJ fluid.

Source	Type[a]	NP[b]	Range T*	Range ρ*	Comments
Levesque and Verlet, 1969 [2]	ST, polynomial	6, 9	1·6–4·6	0·5–0·95	Two different equations of state.
Hansen, 1970 [3]	ST, polynomial	10	2·74–100	liquid-like	Based on inverse-12 potential fluid.
McDonald and Singer, 1972 [4]	E, polynomial	20	0·551–1·237	0·65–0·96	Also contains logarithms of T^* and ρ^*
Nicolas et al., 1979 [5]	E, MBWR	33	0·5–6·0	0–1·2	Critical point too high.
Sýs and Malijevský, 1980 [6]	E, BWR-like	21	0·7–100	0–2	Correlates only pressures, also requires 2nd and 3rd virial coefficients.
Ree, 1980 [7]	ST, polynomial	15	0·8–100	liquid-like	Modification to Hansen's equation.
Adachi et al., 1988 [8]	E, MBWR	33	0·5–6·0	0–1·2	Correlates only pressures.
Nezbeda and Aim, 1989 [9]	ST, polynomial	5	0·72–2·74	0·35–0·85	Correlates only pressures.
Song and Mason, 1989 [10]	ST, integrals of the potential	0	0·75–100	0–2	Only fair agreement with simulation data.
Miyano, 1992 [12]	E, MBWR	33	0·45–100	0·2–1·1	Modification of MBWR to improve high T^* range.

[a] ST = semi-theoretical, E = empirical.
[b] NP = number of adjustable parameters.

expansions about a repulsive reference fluid. Levesque and Verlet [2] were the first to publish an equation of state for the LJ fluid. They presented two semi-theoretical equations based on a λ expansion of the attractive part of the potential [36]. The first and second order perturbation terms were fitted to polynomials in density. Hansen [3] fitted a polynomial for the equation of state for a repulsive r^{-12} potential fluid, and another polynomial for the first order correction term. Ree [7] later modified Hansen's equation by adding a second polynomial for the attractive term that extended the range of applicability. Nezbeda and Aim [9] developed an equation of state based on a first order Weeks–Chandler–Andersen (WCA) perturbation theory [37]. They fitted the attractive term to a polynomial in density and a power-law in temperature. They included pressures, but no internal energies in their regression. Song and Mason [10] developed a WCA-like expansion that depends only on the hard sphere equation of state [38] and three integrals involving the pair potential. Their equation contains no adjustable parameters, but is not as accurate as the other semitheoretical equations.

The strictly empirical equations of state include the following: McDonald and Singer [4], Nicolas *et al.* [5], Sýs and Malijevský [6], Adachi *et al.* [8] and Miyano [12]. Of these, all but McDonald and Singer used some modified form of the Benedict–Webb–Rubin equation. Because we are using the same form as Nicolas *et al.* we will discuss their work in more detail. They used a modification of the Benedict–Webb–Rubin equation of state due to Jacobsen and Stewart [39] that contains 32 linear parameters and one nonlinear parameter. This equation has been the most widely used and arguably the most successful of any yet developed for the LJ fluid. The success of the Nicolas equation is probably due to the wide fluid range that it correlates accurately. The MBWR equation has sufficient flexibility to reproduce the properties of the LJ fluid from low to fairly high temperatures and from gas to liquid densities. The equation contains temperature-dependent expressions to account for the first few virial coefficients. While these expressions are entirely empirical, they can give good results if the parameters are regressed properly. This is an advantage over equations of state based on perturbation theories, which are usually inaccurate for low to moderate densities. The disadvantage of an empirical equation of state is that it is not reliable outside the range for which the parameters were determined, and may even give unphysical results. Nicolas *et al.* regressed the 32 linear parameters based on a data set containing most of the LJ data then published. They also included exact second virial coefficients in the range $0.625 \leq T^* \leq 20$, and 28 low density points generated from the virial series using the first five virial coefficients as calculated by Barker *et al.* [40]. They constrained their linear optimization to ensure that the equation gave critical constants of $T_c^* = 1.35$, $\rho_c^* = 0.35$ and $P_c^* = 0.14$. The nonlinear parameter in the MBWR equation was optimized by a manual 1-dimensional search.

In passing we note that Lotfi *et al.* [11] fitted saturation vapour pressures to a Clausius–Clapeyron equation, and saturation densities to a Guggenheim-like expression [41]. While these equations do not constitute a proper equation of state, they do provide accurate correlations for saturation properties. Lotfi *et al.* also presented a correlation for the saturation chemical potential and the enthalpy of vaporization. The data for these correlations came from their simulations [11].

Table 5. The a_i temperature dependent coefficients for the Helmholtz free energy equation (5). The x_j's are the adjustable parameters in the equation of state.

i	a_i
1	$x_1 T^* + x_2\sqrt{T^*} + x_3 + x_4/T^* + x_5/T^{*2}$
2	$x_6 T^* + x_7 + x_8/T^* + x_9/T^{*2}$
3	$x_{10} T^* + x_{11} + x_{12}/T^*$
4	x_{13}
5	$x_{14}/T^* + x_{15}/T^{*2}$
6	x_{16}/T^*
7	$x_{17}/T^* + x_{18}/T^{*2}$
8	x_{19}/T^{*2}

4. Modified Benedict–Webb–Rubin equation of state

The MBWR equation of state used here is the same as that used by Nicolas *et al.* [5], and contains 32 linear parameters and one nonlinear parameter. We started by writing the expression for the Helmholtz free energy. We worked in reduced units so $A_r^* = A_r/N\epsilon$ where A_r is the residual Helmholtz free energy of the fluid $(A_r(N, V, T) \equiv A(N, V, T) - A_{id}(N, V, T)$, where A_{id} is the ideal gas value). A_r^* is given by

$$A_r^* = \sum_{i=1}^{8} \frac{a_i \rho^{*i}}{i} + \sum_{i=1}^{6} b_i G_i, \tag{5}$$

where the coefficients a_i and b_i are functions of temperature only. These coefficients contain the 32 linear parameters in the MBWR equation. The G_i functions contain exponentials of the density and the one nonlinear parameter. The functional forms of the a_i, b_i, and G_i are given in tables 5, 6 and 7, respectively. From equation (5) we can derive all other thermodynamic properties. The pressure is given by

$$P^* = \rho^* T^* + \rho^{*2} \left(\frac{\partial A_r^*}{\partial \rho^*} \right)_{T^*, N}, \tag{6}$$

where $P^* = P\sigma^3/\epsilon$ includes the ideal gas contribution. Substituting equation (5) into equation (6) gives

Table 6. The b_i temperature dependent coefficients for the Helmholtz free energy equation (5). The x_j's are the adjustable parameters in the equation of state.

i	b_i
1	$x_{20}/T^{*2} + x_{21}/T^{*3}$
2	$x_{22}/T^{*2} + x_{23}/T^{*4}$
3	$x_{24}/T^{*2} + x_{25}/T^{*3}$
4	$x_{26}/T^{*2} + x_{27}/T^{*4}$
5	$x_{28}/T^{*2} + x_{29}/T^{*3}$
6	$x_{30}/T^{*2} + x_{31}/T^{*3} + x_{32}/T^{*4}$

Table 7. The G_i density dependent coefficients for the Helmholtz free energy equation (5), where $F = \exp(-\gamma\rho^{*2})$, and γ is the nonlinear adjustable parameter. We have chosen $\gamma = 3$ in this work.

i	G_i
1	$(1 - F)/(2\gamma)$
2	$-(F\rho^{*2} - 2G_1)/(2\gamma)$
3	$-(F\rho^{*4} - 4G_2)/(2\gamma)$
4	$-(F\rho^{*6} - 6G_3)/(2\gamma)$
5	$-(F\rho^{*8} - 8G_4)/(2\gamma)$
6	$-(F\rho^{*10} - 10G_5)/(2\gamma)$

$$P^* = \rho^* T^* + \sum_{i=1}^{8} a_i \rho^{*(i+1)} + F \sum_{i=1}^{6} b_i \rho^{*(2i+1)}, \qquad (7)$$

where $F = \exp(-\gamma\rho^{*2})$, γ is the nonlinear adjustable parameter, and the coefficients a_i and b_i are the same functions that appear in the Helmholtz free energy expression of equation (5). The residual (configurational) internal energy $U_r^* = U_r/N\epsilon$ is given by

$$U_r^* = -T^{*2} \left(\frac{\partial(A_r^*/T^*)}{\partial T^*} \right)_{\rho*, N}. \qquad (8)$$

Using equation (5) in equation (8) gives

$$U_r^* = \sum_{i=1}^{8} \frac{c_i \rho^{*i}}{i} + \sum_{i=1}^{6} d_i G_i, \qquad (9)$$

where the coefficients c_i and d_i are given in tables 8 and 9, and the G_i functions are given in table 7. One final property is the Gibbs free energy per atom which, for the pure fluid case, is equal to the chemical potential:

$$G_r^* = \frac{G_r}{N\epsilon} = \mu_r^* = A_r^* + \frac{P^*}{\rho^*} - T^*, \qquad (10)$$

where A_r^* is given by equation (5) and P^* is given by equation (7).

Table 8. The c_i temperature dependent coefficients for the internal energy equation (8). The x_j's are the adjustable parameters in the equation of state.

i	c_i
1	$x_2\sqrt{T^*}/2 + x_3 + 2x_4/T^* + 3x_5/T^{*2}$
2	$x_7 + 2x_8/T^* + 3x_9/T^{*2}$
3	$x_{11} + 2x_{12}/T^*$
4	x_{13}
5	$2x_{14}/T^* + 3x_{15}/T^{*2}$
6	$2x_{16}/T^*$
7	$2x_{17}/T^* + 3x_{18}/T^{*2}$
8	$3x_{19}/T^{*2}$

Table 9. The d_i temperature dependent coefficients for the internal energy equation (8). The x_j's are the adjustable parameters in the equation of state.

i	d_i
1	$3x_{20}/T^{*2} + 4x_{21}/T^{*3}$
2	$3x_{22}/T^{*2} + 5x_{23}/T^{*4}$
3	$3x_{24}/T^{*2} + 4x_{25}/T^{*3}$
4	$3x_{26}/T^{*2} + 5x_{27}/T^{*4}$
5	$3x_{28}/T^{*2} + 4x_{29}/T^{*3}$
6	$3x_{30}/T^{*2} + 4x_{31}/T^{*3} + 5x_{32}/T^{*4}$

4.1. *Regression of parameters*

We have constrained the equation of state to give a specified critical temperature and density. The MBWR equation is classical and gives a critical exponent of 1/2. Thus, it is incapable of giving a $\rho-T$ critical region that is sufficiently flat. Even so, it is important for the equation to give good values of the critical constants. The early estimates for the critical constants [13] were $T_c^* = 1\cdot36 \pm 0\cdot04$ and $\rho_c^* = 0\cdot31 \pm 0\cdot03$. Later, Adams [27] estimated $T_c^* = 1\cdot30 \pm 0\cdot02$ and $\rho_c^* = 0\cdot33 \pm 0\cdot03$. Smit [20, 21] gave estimates based on fitting Gibbs ensemble data to the critical scaling law for density and to the law of rectilinear diameters. His estimates are $T_c^* = 1\cdot316 \pm 0\cdot006$ and $\rho_c^* = 0\cdot304 \pm 0\cdot006$. Smit used the 3-dimensional critical exponent, $\beta = 0\cdot32$, in his fitting procedure. Lotfi *et al.* [11] made estimates of $T_c^* = 1\cdot31$ and $\rho_c^* = 0\cdot314$ based on their VLE data for the LJ fluid. They did not use the law of rectilinear diameters to determine the critical density; however, their data follow a line of rectilinear diameters extremely well. Applying the law of rectilinear diameters to their data gives $\rho_c^* = 0\cdot310$, slightly lower than the value of $0\cdot314$ they report. If we plot the Gibbs ensemble data on the same plot as the data of Lotfi *et al.* we notice that the low temperature Gibbs ensemble data fall on the same line of rectilinear diameters as the data of Lotfi *et al.* The Gibbs ensemble data for $T^* = 1\cdot25$ and above deviate from the Lotfi *et al.* data, but the uncertainties in the Gibbs ensemble data are also large, so that the data agree to within the estimated errors. We have chosen to use $\rho_c^* = 0\cdot310$ and $T_c^* = 1\cdot313$ as the best estimates for the critical density and temperature in our equation of state. The critical temperature used is an average of the estimates from the Gibbs ensemble data and from Lotfi's data. The value of ρ_c^* depends on T_c^* through the line of rectilinear diameters. However, using the slope from the Lotfi *et al.* data we find that to three significant figures the value of ρ_c^* does not change in going from a critical temperature of $1\cdot310$ to $1\cdot313$. The constraints for the critical point are

$$\left(\frac{\partial P}{\partial \rho}\right)_T \bigg|_{T_c, \rho_c} = 0, \tag{11}$$

and

$$\left(\frac{\partial^2 P}{\partial \rho^2}\right)_T \bigg|_{T_c, \rho_c} = 0. \tag{12}$$

We have not specified a value of the critical pressure in the fitting procedure because P_c^* is not known accurately from simulations. Given the above values of T_c^* and ρ_c^*,
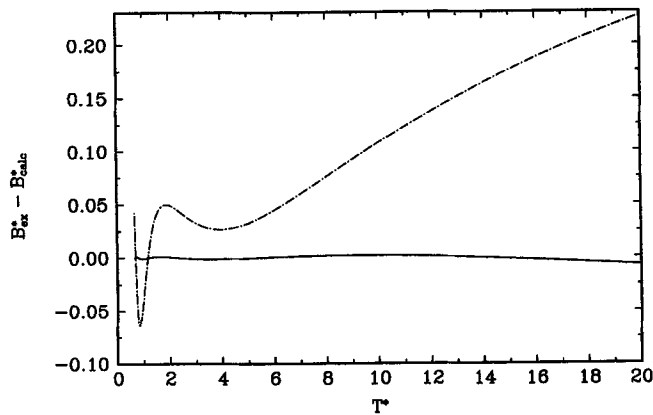
Figure 2. The deviation plot for the reduced second virial coefficient, $B^* = 3B/(2\pi\sigma^3)$, as correlated by the new MBWR parameters (solid line) and the original Nicolas *et al.* parameters (dot-dashed line). B_{ex}^* is the exact second virial coefficient.

the equation of state with the new parameters gives $P_c^* = 0.13$.

The first five parameters in the MBWR equation (x_1-x_5) determine the second virial coefficient. We have generated exact second virial coefficients at 315 temperatures in the range $0.66 \leq T^* \leq 20$ and have used these data to determine the first five parameters in the MBWR equation. We show the deviation plots for the second virial coefficient from our new parameters and the original Nicolas *et al.* parameters in figure 2. The new parameters correlate the second virial coefficient over a wide temperature range with much higher accuracy than the Nicolas *et al.* parameters.

After specifying the five parameters in the second virial coefficient correlation (x_1-x_5) we are left with 27 linear parameters and one nonlinear parameter to fit. We have used the molecular dynamics data listed in table 2 to regress these parameters. We weighted the data with the reciprocal of the uncertainties for both the pressures

Table 10. New parameters for the modified Benedict–Webb–Rubin equation of state regressed from the simulation data of this work.

j	x_j	j	x_j
1	0·862 308 509 750 742 1	17	6·398 607 852 471 505e + 01
2	2·976 218 765 822 098	18	1·603 993 673 294 834e + 01
3	−8·402 230 115 796 038	19	6·805 916 615 864 377e + 01
4	0·105 413 662 920 355 5	20	−2·791 293 578 795 945e + 03
5	−0·856 458 382 817 459 8	21	−6·245 128 304 568 454
6	1·582 759 470 107 601	22	−8·116 836 104 958 410e + 03
7	0·763 942 194 830 545 3	23	1·488 735 559 561 229e + 01
8	1·753 173 414 312 048	24	−1·059 346 754 655 084e + 04
9	2·798 291 772 190 376e + 03	25	−1·131 607 632 802 822e + 02
10	−4·839 422 026 085 765 7e − 02	26	−8·867 771 540 418 822e + 03
11	0·996 326 519 772 193 5	27	−3·986 982 844 450 543e + 01
12	−3·698 000 291 272 493e + 01	28	−4·689 270 299 917 261e + 03
13	2·084 012 299 434 647e + 01	29	2·593 535 277 438 717e + 02
14	8·305 402 124 717 285e + 01	30	−2·694 523 589 434 903e + 03
15	−9·574 799 715 203 068e + 02	31	−7·218 487 631 550 215e + 02
16	−1·477 746 229 234 994e + 02	32	1·721 802 063 863 269e + 02
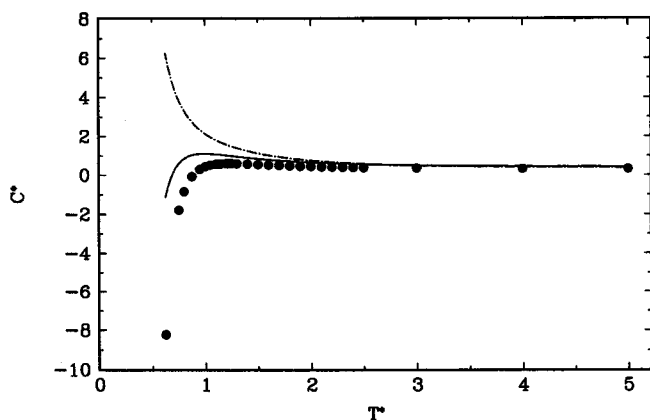
Figure 3. The pairwise-additive reduced third virial coefficient, $C^* = (3/(2\pi\sigma^3))^2 C$, from the exact calculations of Barker *et al.* [40] (●), the new MBWR parameters (solid line), and the Nicolas *et al.* parameters (dot-dashed line).

and internal energies listed in table 2. For the $\rho^* = 0.005$ densities with two independent runs we used the average value of the runs and the sample standard deviation calculated from the two observed points.

We attempted to fit simultaneously the nonlinear parameter γ and the 27 remaining linear parameters by using the Minpack nonlinear optimization package [42]. However, including γ in the fit made the problem ill-conditioned, and Minpack was not able to find a global minimum. As a result, we regressed the linear parameters at various fixed values of γ for $1 \leq \gamma \leq 7$. We observed that the minimum is a very weak function of γ, in agreement with the findings of Nicolas *et al.* [5]. A shallow minimum from this search routine occurred near $\gamma = 3.5$. However, we have chosen to retain the value $\gamma = 3$ for historical reasons. This does not appreciably affect the accuracy of fit. The final values of the parameters are given in table 10. The fit to the simulation data is very good over most of the $T^*-\rho^*$ plane. The average absolute deviations (AAD) are 0.017 in P^* and 0.016 in U^*. Most of the error for both pressure and internal energy occurs in the region of high temperature and high density, $T^* > 4.0$ and $\rho^* > 1.0$.

The value of χ^2/N_f for this fit is 37.2, where

$$\chi^2 = \sum_{i=1}^{N_p} \frac{(X_i^{\text{sim}} - X_i^{\text{calc}})^2}{S_i^2}, \tag{13}$$

X_i^{sim} is the value of either P^* or U^* from simulation, and X_i^{calc} is the corresponding value from the equation of state. S_i is the sample error of the mean as calculated from the simulations, the sum is over the number of points N_p, and N_f is the number of degrees of freedom, where $N_f = 356 - 27 = 329$ in this case.

The reduced third virial coefficient, $C^* = (3/(2\pi\sigma^3))^2 C$, is shown in figure 3. While no C^* data were directly used in the parameter regression of either Nicolas *et al.* or this work, we see that the new parameters give qualitatively correct temperature dependence of the third virial coefficient. The Nicolas *et al.* parameters give the wrong qualitative temperature dependence for $T^* < 2.5$. Because this is the temperature region important for VLE, we expect the new parameters to give better saturated vapour densities and energies.

J. K. Johnson *et al.*
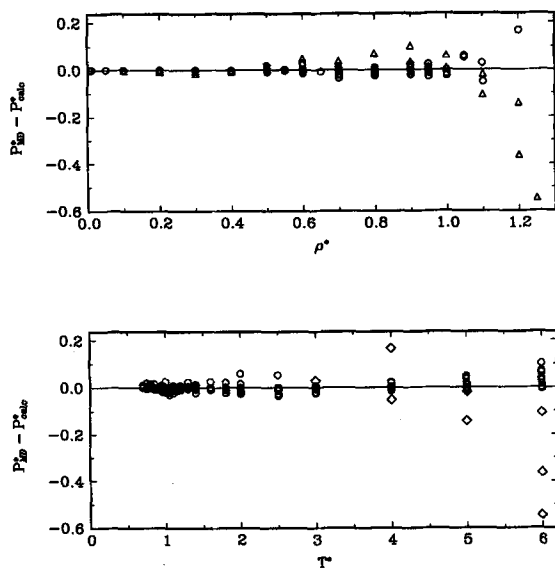
Figure 4. The deviation plots for pressure, where P^*_{MD} denotes the simulation results of this work and P^*_{calc} denotes the equation of state calculations with the new MBWR parameters. In the upper figure the triangles are for $T^* \geq 5$. In the lower figure the diamonds are for $\rho^* \geq 1 \cdot 1$.
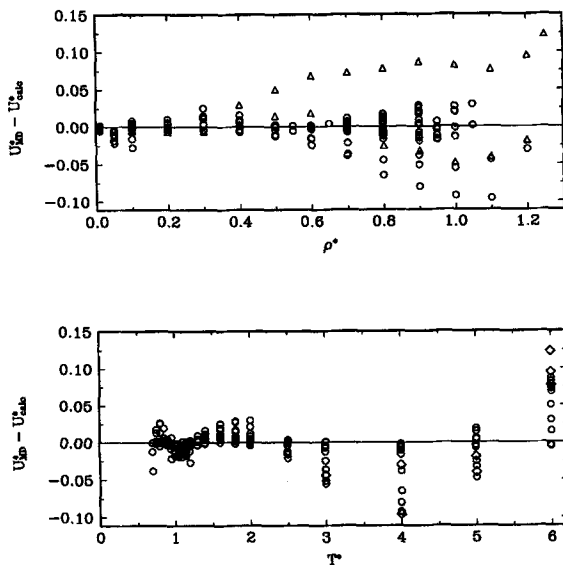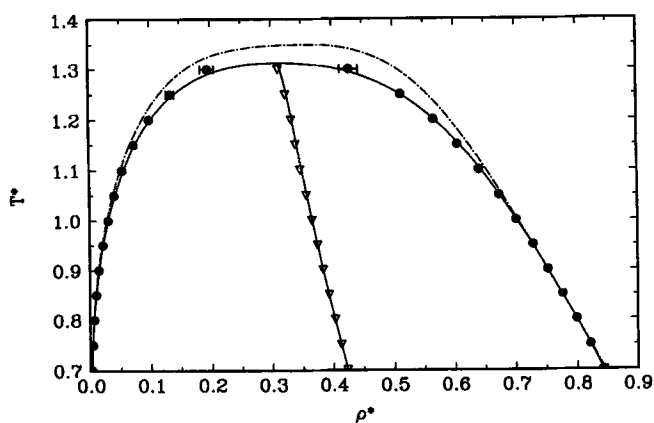

Figure 5. The deviation plots for internal energy, where U^*_{MD} denotes the simulation results of this work and U^*_{calc} denotes the equation of state calculations with the new MBWR parameters. In the upper figure the triangles are for $T^* \geq 5$. In the lower figure the diamonds are for $\rho^* \geq 1 \cdot 1$.

Figure 6. Saturation densities from the simulations of Lotfi *et al.* [11] (solid circles), and predictions from the equation of state using the new MBWR parameters (solid line), and the Nicolas *et al.* parameters (dot-dashed line). The line of rectilinear diameters is also shown for the simulation results (triangles) and from the equation of state using the new MBWR parameters (solid line).

In figure 4 we show the deviations for the pressure, $P^*_{MD} - P^*_{calc}$, where P^*_{MD} denotes the MD simulation results, and P^*_{calc} is calculated from the equation of state. The largest errors occur at the highest temperatures and densities. The equation of state does not fit this region particularly well, and one should keep this in mind if properties of the high temperature dense fluid are needed. However, even at the highest absolute error the relative error is only -0.6%, because at this point $P^* = 85.7$. This corresponds to a pressure of about 3.4 GPa for methane. The errors in the internal energy are shown in figure 5. The errors are again largest for the high temperature, high density points. It is apparent from figure 5 that the deviations are not random, but systematic. This indicates that the equation of state is not capable of fitting both the vapour–liquid region and high temperature region with comparable accuracy. Although this highlights the shortcomings of the MBWR equation of state, we stress that these errors are still only a few percent at worst.
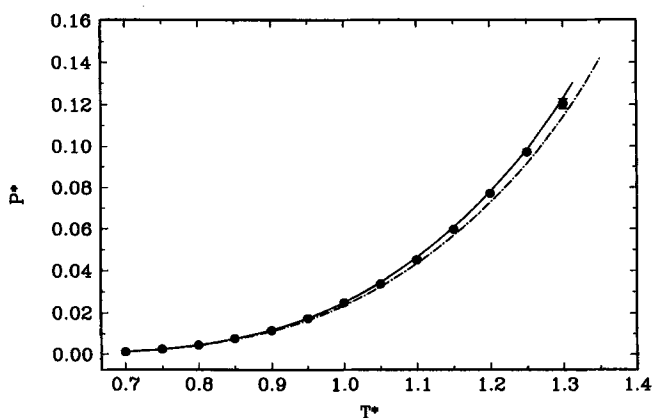
Figure 7. Saturation vapour pressure curve from the data of Lotfi *et al.* [11] (points), and predictions from the equation of state using the new MBWR parameters (solid line), and the Nicolas *et al.* parameters (dot-dashed line).
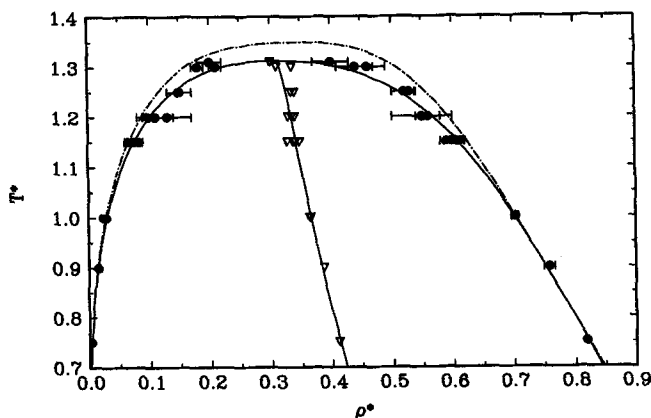
Figure 8. Saturation densities from the Gibbs ensemble simulations reported in reference [20] (solid circles), and predictions from the equation of state using the new MBWR parameters (solid line), and the Nicolas *et al.* parameters (dot-dashed line). The line of rectilinear diameters is also shown for the simulation results (triangles) and from the equation of state using the new MBWR parameters (solid line).

The predicted VLE data are compared with data from simulations in figures 6–9. In figures 6 and 7 we see the predictions compared with the VLE data of Lotfi *et al.* Figure 6 shows the $T^*-\rho^*$ projection. We see that the new parameters accurately predict both the vapour and liquid orthobaric densities from about the triple point to close to the critical point. The original Nicolas *et al.* parameters are quite accurate at low temperatures, but for $T^* > 1$ the new parameters are significantly more accurate. Figure 7 shows the vapour pressure curve for the LJ fluid. From this figure we see that the new parameters accurately predict the saturated vapour pressures up to the critical point. In figures 8 and 9 we present VLE calculations compared with Gibbs ensemble simulations. The Gibbs ensemble data were taken from the compilation in [20]. We see the same results as in figures 6 and 7, except that the Gibbs ensemble data show more scatter, especially at high temperatures. The new
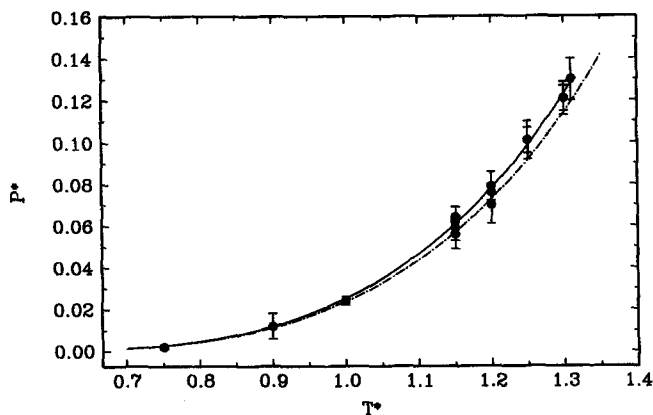
Figure 9. Saturation vapour pressure curve from the Gibbs ensemble data reported in reference [20] (points), and predictions from the equation of state using the new MBWR parameters (solid line), and the Nicolas *et al.* parameters (dot-dashed line).
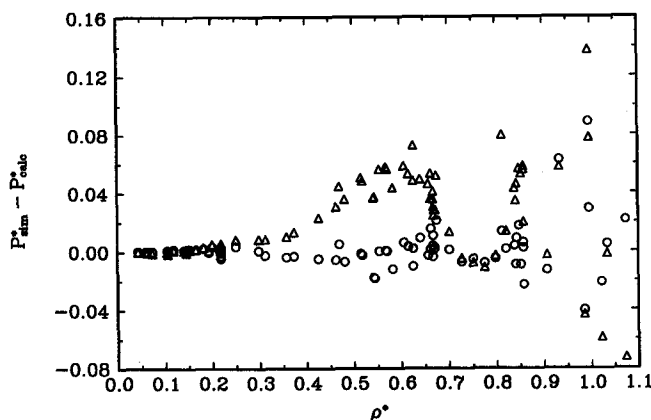
Figure 10. The difference plot for pressure, where P_{sim}^* are the pressures from references [11, 27, 30], and P_{calc}^* is calculated from the MBWR equation of state using the new parameters (circles) and the Nicolas *et al.* parameters (triangles). None of these data was used in the regression of either the new or the Nicolas *et al.* parameters. The data cover the temperature range $0.7 \leq T^* \leq 4.0$, with most of the data being at the lower temperatures.

parameters also give fairly good agreement with the older VLE data from the grand canonical simulations of Adams [17, 27]. Although the new equation is more accurate than that of Nicolas *et al.* for VLE calculations, the accuracy of the new equation is somewhat lower for dense fluids at temperatures greater than twice the critical.

We have compared calculations from the new equation with many of the literature data reviewed in section 2.1. In making the comparison, we have excluded data that were outside the fitting range of the new parameters. We find that the newer data [11, 27, 29, 30], which were not included in fitting the Nicolas *et al.* equation, are in better agreement with the new equation than with that of Nicolas *et al.* An exception is the data set of Shaw [29], which includes many points in the high temperature, high density range, where the new equation presented here does not perform particularly well. The deviation plots for the pressure data of [11, 27, 30] are shown in figure 10. On the whole, the new parameters give a better representation of the data than the parameters of Nicolas *et al.*

Schmidt and Wagner [43] developed a MBWR equation for correlating the properties of oxygen and other real fluids. Like the Jacobsen–Stewart MBWR equation used by Nicolas *et al.*, the Schmidt–Wagner (SW) equation contains 32 linear parameters for the residual Helmholtz free energy. However, the terms in the SW equation were selected to give the most efficient representation of experimental data over a limited range. We regressed the parameters in the SW equation from the full LJ data of table 2, but found that the fit was much worse than that of the MBWR equation presented above. We reduced our data set to include only points that were within the reduced pressure range used by Schmidt and Wagner [43] to develop the functional form of their equation ($P < 20P_c$). However, the χ^2 of the fit to the SW equation was still about three times that of the Jacobsen–Stewart MBWR equation fitted to the same range. We conclude that the equation used by Nicolas *et al.* is better than the SW equation for correlating thermodynamic data for the LJ fluid.

5.   MBWR for the cut and shifted potential

In table 2 we presented simulation results for both the full LJ fluid and the cut and shifted fluid corresponding to the potential of equation (4). In this section we present an equation of state for the cut and shifted fluid that is based on a simple mean-field correction of the full LJ equation of state presented in section 4.

Powles [44] derived approximate corrections for transforming from the pressure of the full LJ fluid to that of the cut and shifted, and shifted-force fluids. He applied this correction to the Nicolas *et al.* equation and compared his calculations with a few simulation results for the cut and shifted, and shifted-force potentials. He found good agreement for the cut and shifted fluid. In this section we present a rigorous derivation for the corrections to the Helmholtz free energy, the pressure, and the internal energy.

The change in the Helmholtz free energy due to a change in the potential can be written as a functional derivative [45],

$$\frac{\delta A}{\delta \phi} = \rho^2 g(r_1, r_2), \tag{14}$$

where $g(r_1, r_2)$ is the pair correlation function, r_i is the vector defining the position of atom i, and $\delta\phi$ is the change in the pair potential. For the change in going from the full LJ potential to the cut and shifted potential

$$\delta\phi(r) = \phi_{cs}(r) - \phi(r) = \begin{cases} -\phi(r_c) & \text{if } r < r_c \\ -\phi(r) & \text{if } r > r_c \end{cases}, \tag{15}$$

where $\phi(r)$ is the full LJ potential given by equation (1), $\phi_{cs}(r)$ is the cut and shifted potential given by equation (4), and r_c is the potential cutoff. The change in Helmholtz energy is

$$A_{cs} - A = 2\pi N\rho \int_0^\infty g(r)\delta\phi(r)r^2 \mathrm{d}r \tag{16}$$
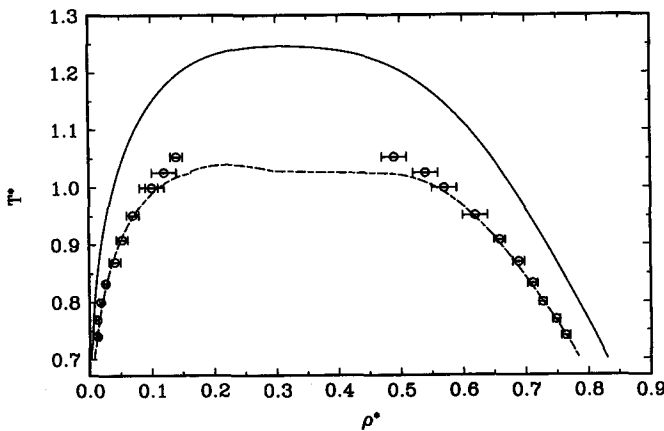
Figure 11. Saturation densities for two different cut and shifted fluids. The lines are from the equation using the mean-field corrections, equations (18) and (19). The solid line is for the cut and shifted fluid with $r_c = 4\sigma$. The points and the dashed line are for the cut and shifted fluid with $r_c = 2 \cdot 5\sigma$. The points are the Gibbs ensemble data of Smit [20] and the dashed line is from the equation of state using the mean-field corrections.
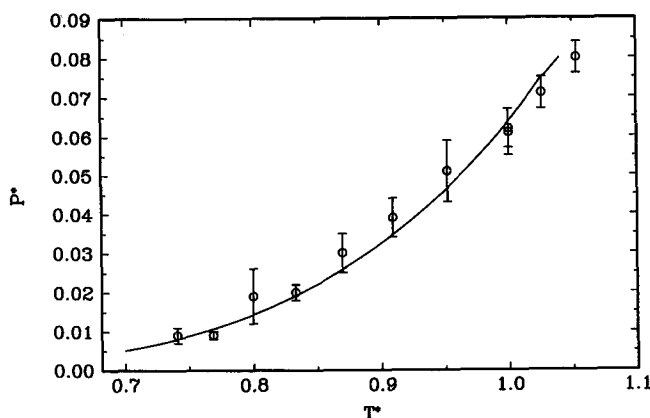
Figure 12. The vapour pressure curve for the cut and shifted fluid with $r_c = 2.5\sigma$. The points are the Gibbs ensemble simulations of Smit [20], and the line is calculated from the equation using the mean-field corrections to the cut and shifted fluid.

$$= -2\pi N\rho \left[\phi(r_c) \int_0^{r_c} g(r)r^2 dr + \int_{r_c}^{\infty} g(r)\phi(r)r^2 dr \right], \tag{17}$$

where equation (15) has been used for $\delta\phi(r)$. Next we introduce two approximations. We first assume that $g(r) = 1$ for $r > r_c$. Next we notice that $2\pi\rho \int_0^{r_c} g(r)r^2 dr$ in equation (17) is just the number of pairs of atoms within the cutoff of a central atom. We approximate this by the average number of pairs of atoms in the volume of a sphere of radius r_c. This leads directly to

$$A_{cs}^* - A^* = -\frac{32}{9}\pi\rho^* \left[\left(\frac{\sigma}{r_c}\right)^9 - \frac{3}{2}\left(\frac{\sigma}{r_c}\right)^3 \right]. \tag{18}$$

We can calculate the correction to the internal energy by substituting equation (18) into equation (8); it is exactly equal to the right hand side of equation (18).
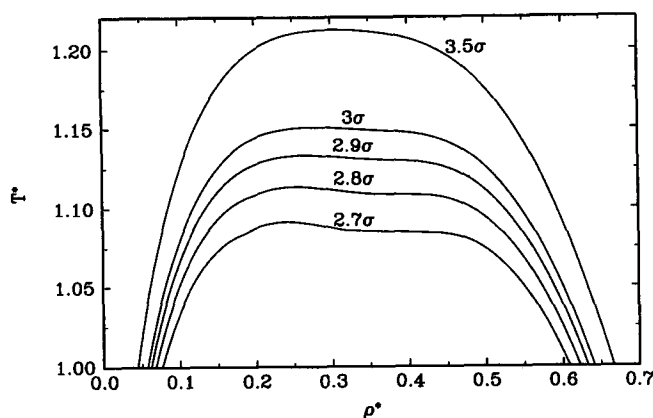
Figure 13. Saturated densities in the critical region from the mean-field approach, equations (18) and (19), for the cut and shifted fluid at several different values of the cutoff, r_c.

The pressure correction is calculated from equations (18) and (6) and is given by

$$P_{cs}^* - P^* = -\frac{32}{9}\pi\rho^{*2}\left[\left(\frac{\sigma}{r_c}\right)^9 - \frac{3}{2}\left(\frac{\sigma}{r_c}\right)^3\right].\qquad(19)$$

These two approximations are made in the spirit of mean-field theory, and therefore we refer to equations (18) and (19) as the mean-field corrections for the cut and shifted fluid. Note that equation (19) is the same as equation (2) for the tail correction to the pressure except for the sign. This is because the shift in the potential does not affect the pressure. The correction to the energy is not the same as the tail, equation (3), because the energy depends on contributions form both the potential shift and the cutoff. We have applied these corrections to the full MBWR equation of state and compared predictions from this new equation of state with the cut and shifted simulation data of table 2. We find that calculations from the mean-field equations for the cut and shifted fluid are about as accurate as the fit to the full LJ data. The AAD for P^* is 0·017 and for U^* the AAD is 0·016, and the value of χ^2/N_f is 34·4, for $N_f = 356$, which indicates that the mean-field approximations are very accurate for this cutoff. The critical properties predicted from equation (19) are $T_c^* = 1·246$, $\rho_c^* = 0·308$ and $P_c^* = 0·118$, for $r_c = 4\sigma$.

This mean-field approach is not limited to a cutoff of 4σ, of course. The same equations may be applied to any cutoff. However, the accuracy of both approximations will deteriorate as r_c becomes smaller. In figure 11 we present the T^*–ρ^* projection of the vapour–liquid phase diagram for the cut and shifted fluid for two different values of r_c. The solid line was calculated from the mean-field approach with $r_c = 4\sigma$, while the dashed line is for $r_c = 2·5\sigma$. The points are the Gibbs ensemble results of Smit [20] with $r_c = 2·5\sigma$. We see that the mean-field approach gives very good agreement with the Gibbs ensemble results for $T^* < 1$, but the equation of state predicts a lower critical temperature and exhibits an unphysical hump in the phase diagram near the critical point, as was noted by Smit [20, 21]. Figure 12 shows the vapour pressure plot for the cut and shifted fluid with $r_c = 2·5\sigma$ from the equation of state and from simulations. The mean-field approach predicts the saturation pressures to within the accuracy of the simulations, except near the critical point. The unphysical hump in the phase dome may be related to a problem noted by Reddy and O'Shea [46], who regressed parameters for the MBWR equation of state from data for the 2-dimensional LJ fluid. They did not fix the values of the critical temperature and density in fitting the parameters, and found that the resulting equation had three solutions for the critical conditions (11) and (12). We have searched for the critical points of the MBWR equation using a nonlinear root finding routine to solve equations (11) and (12) by starting from various initial guesses. For $r_c = 2·5\sigma$ the equation predicts three critical points, the (T^*, ρ^*) coordinates of which are (0·7248, 0·3432), (1·0017, 0·329), and (1·0399, 0·2215). These last two critical points are very close, and are perhaps responsible for the unphysical region in the phase diagram. We have tested the limit of applicability of the mean-field equation by examining the saturation densities in the critical region for various values of r_c (figure 13). We find that the unphysical hump begins to appear around $r_c = 2·9\sigma$, and therefore conclude that the mean-field equations for the cut and shifted fluid should give reasonable results for $r_c > 3\sigma$.
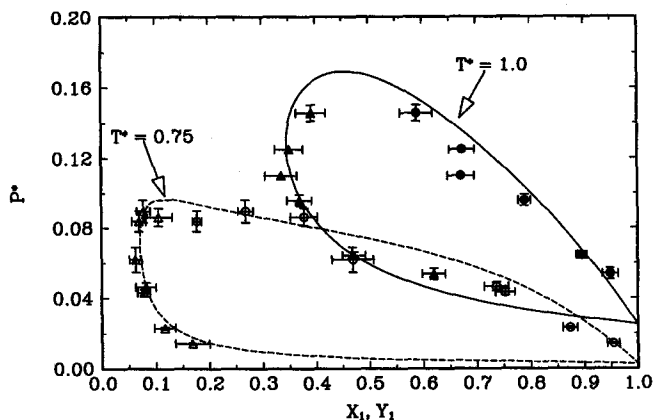
Figure 14. Vapour–liquid equilibrium calculations for LJ mixtures from the Gibbs ensemble simulations of reference [49] (points) and from the equation of state with new parameters (lines). The LJ parameters are $\epsilon_{22}/\epsilon_{11} = 0.5$ and $\sigma_{22}/\sigma_{11} = 1$. The Lorentz-Berthelot combining rules are used for the cross-interactions.

6. Extension to mixtures

The MBWR equation was developed for pure fluids. Any attempt to apply this equation to mixtures must include some approximate theory such as the conformal solution theory or corresponding states [47]. The most successful conformal solution theory is the van der Waals one-fluid theory (vdW1). The vdW1 theory is capable of predicting accurately the behaviour of fluid mixtures if the difference in size or energy parameters is not too large. Shing and Gubbins [48] found that vdW1 gives good results for Henry's law constants when the difference in the LJ size parameter is not more than about 10%. Harismiadis *et al.* [49] found fairly good results using vdW1 for phase equilibrium calculations of binary LJ mixtures, even when both the size and energy parameters differed by a factor of 2. Their results suggest that phase
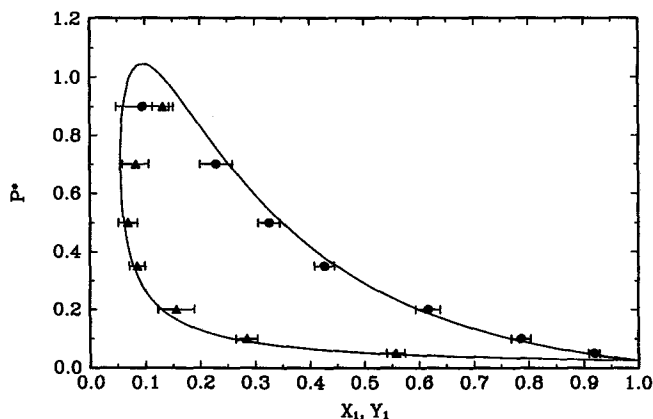

Figure 15. Vapour–liquid equilibrium calculations for LJ mixtures from the Gibbs ensemble simulations of reference [49] (points) and from the equation of state with new parameters (line). The LJ parameters are $\epsilon_{22}/\epsilon_{11} = 0.5$ and $\sigma_{22}/\sigma_{11} = 0.5$. The Lorentz-Berthelot combining rules are used for the cross-interactions.

equilibrium calculations are less sensitive to mixing rules than excess properties or infinite dilution chemical potentials.

The vdW1 mixing rules for the LJ fluid are

$$\sigma_x^3 = \sum_i \sum_j X_i X_j \sigma_{ij}^3, \tag{20}$$

and

$$\epsilon_x = \frac{1}{\sigma_x^3} \sum_i \sum_j X_i X_j \epsilon_{ij} \sigma_{ij}^3, \tag{21}$$

where the subscript x denotes the mixture property and X_i is the mole fraction of component i in the mixture. The cross-interaction parameters ϵ_{ij} and σ_{ij} are often chosen by some kind of combining rules, e.g., Lorentz–Berthelot.

The MBWR equation of state used in this work gives the Helmholtz free energy as a function of ρ^* and T^*. For mixtures we use the same functional form, but the independent variables become composition-dependent through $\rho^* = \rho \sigma_x^3$ and $T^* = kT/\epsilon_x$. The reduced thermodynamic properties are also explicitly composition-dependent: $A_r^* = A_r/N\epsilon_x$, $P^* = P\sigma_x^3/\epsilon_x$, and $U_r^* = U/N\epsilon_x$. The chemical potential for component i in the mixture can be calculated from

$$\mu_{r,i} = \left(\frac{\partial A_r}{\partial N_i}\right)_{T,V,N_{j\neq i}} = \left(\frac{\partial (NA_r^*\epsilon_x)}{\partial N_i}\right)_{T,V,N_{j\neq i}}$$

$$= A_r^*\epsilon_x + A_r^*\rho\left(\frac{\partial \epsilon_x}{\partial \rho_i}\right)_{T,\rho_{j\neq i}} + \rho\epsilon_x\left(\frac{\partial A_r^*}{\partial \rho_i}\right)_{T,\rho_{j\neq i}}. \tag{22}$$

The partial derivatives require derivatives of the mixing rules.

$$\left(\frac{\partial \epsilon_x}{\partial \rho_i}\right)_{T,\rho_{j\neq i}} = -\frac{\epsilon_x}{\sigma_x^3}\left(\frac{\partial \sigma_x^3}{\partial \rho_i}\right)_{T,\rho_{j\neq i}} + \frac{2}{\rho}\left[\frac{1}{\sigma_x^3}\sum_k X_k \epsilon_{ik}\sigma_{ik}^3 - \epsilon_x\right], \tag{23}$$

where

$$\left(\frac{\partial \sigma_x^3}{\partial \rho_i}\right)_{T,\rho_{j\neq i}} = \frac{2}{\rho}\left[\sum_k X_k \sigma_{ik}^3 - \sigma_x^3\right]. \tag{24}$$

The last term in equation (22) simplifies after some algebra to

$$\left(\frac{\partial A_r^*}{\partial \rho_i}\right)_{T,\rho_{j\neq i}} = \left(\frac{P^*}{\rho^{*2}} - \frac{T^*}{\rho^*}\right)\left[\sigma_x^3 + \rho\left(\frac{\partial \sigma_x^3}{\partial \rho_i}\right)_{T,\rho_{j\neq i}}\right] - \frac{(A_r^* - U_r^*)}{\epsilon_x}\left(\frac{\partial \epsilon_x}{\partial \rho_i}\right)_{T,\rho_{j\neq i}}. \tag{25}$$

Note that equations (22–25) contain both reduced (ρ^*) and unreduced (ρ) densities.

We have performed phase equilibrium calculations for three binary LJ mixtures and compared the results with Gibbs ensemble simulation data from reference [49]. In figure 14 we present the data for a mixture with the LJ parameters $\epsilon_{22} = 0.5\epsilon_{11}$ and $\sigma_{22} = \sigma_{11}$. The Lorentz–Berthelot combining rules were used for the cross-parameters. The agreement between simulation and the equation of state is generally quite good. The predicted critical points are somewhat too high in pressure, and the liquid phase mole fractions are also high. The P, X, Y diagram for the system with $\epsilon_{22} = 0.5\epsilon_{11}$ and $\sigma_{22} = 0.5\sigma_{11}$ is shown in figure 15. Even for this highly asymmetric mixture the vdW1 mixing rules give surprisingly good results for the pressure and mole fractions.

7. Conclusion

We have presented accurate new MD simulation results for the LJ fluid at 175 different state points over a wide range of temperature and density, together with a few MC simulation data.

Parameters for the MBWR equation of state for the LJ fluid have been regressed for the temperature range $0 \cdot 7 \leq T^* \leq 6$ and covering the entire fluid range of densities. The equation is especially accurate for vapour–liquid equilibrium calculations. Agreement for saturated densities and vapour pressures is seen with Gibbs ensemble, NPT + particle insertion, and grand canonical Monte Carlo simulations. Because we have no more parameters at our disposal than did Nicolas *et al.*, this improved accuracy for phase equilibrium calculations has come at the expense of some loss of accuracy for liquid states at sub-triple point temperatures and at high temperatures ($T^* > 4$) and high densities ($\rho^* > 1 \cdot 0$).

We have presented an equation of state for the cut and shifted fluid that is based on a mean-field correction to the equation of state for the full LJ fluid. This method is applicable for any cutoff; however, the accuracy decreases as the cutoff decreases. For values of $r_c < 3\sigma$ the equation fails to give physically meaningful results in the critical region.

We have performed calculations for various LJ binary mixtures with the van der Waals one-fluid theory, using the MBWR equation for the reference fluid. These calculated values have been compared with Gibbs ensemble simulation data. Predictions from the equation of state are in quite good agreement with the simulation results for the pressures and compositions.

References

[1] MAITLAND, G. C., RIGBY, M., SMITH, E. B., and WAKEHAM, W. A., 1981, *Intermolecular Forces* (Clarendon Press).
[2] LEVESQUE, D., and VERLET, L., 1969, *Phys. Rev.*, **182**, 307.
[3] HANSEN, J.-P., 1970, *Phys. Rev. A*, **2**, 221.
[4] McDONALD, I. R., and SINGER, K., 1972, *Molec. Phys.*, **23**, 29.
[5] NICOLAS, J. J., GUBBINS, K. E., STREETT, W. B. and TILDESLEY, D. J., 1979, *Molec. Phys.*, **37**, 1429.
[6] SÝS, J., and MALIJEVSKÝ, A., 1980, *Collec. Czech. Chem. Commun.*, **45**, 977.
[7] REE, F. H., 1980, *J. chem. Phys.*, **73**, 5401.
[8] ADACHI, Y., FIJIHARA, I., TAKAMIYA, M., and NAKANISHI, K., 1988, *Fluid Phase Equilibria*, **39**, 1.
[9] NEZBEDA, I., and AIM, K., 1989, *Fluid Phase Equilibria*, **52**, 39.
[10] SONG, Y., MASON, E. A., 1989, *J. chem. Phys.*, **91**, 7840.
[11] LOTFI, A., VRABEC, J. and FISCHER, J., 1992, *Molec. Phys.*, **76**, 1319.
[12] MIYANO, Y., 1992, *Fluid Phase Equilibria*, in press.
[13] VERLET, L., 1967, *Phys. Rev.*, **159**, 98.
[14] HANSEN, J.-P., and VERLET, L., 1969, *Phys. Rev.*, **184**, 151.
[15] VERLET, L., and WEIS, J.-J., 1972, *Phys. Rev. A*, **5**, 939.
[16] ADAMS, D. J., 1975, *Molec. Phys.*, **29**, 307.
[17] ADAMS, D. J., 1976, *Molec. Phys.*, **32**, 647.
[18] PANAGIOTOPOULOS, A. Z., 1987, *Molec. Phys.*, **61**, 813.

[19] PANAGIOTOPOULOS, A. Z., QUIRKE, N., STAPLETON, M., and TILDESLEY, D. J., 1988, *Molec. Phys.*, **63**, 527.
[20] SMIT, B., 1990, Ph.D. Dissertation, University of Utrecht, The Netherlands.
[21] SMIT, B., 1992, *J. chem. Phys.*, **96**, 8639.
[22] SMIT, B., DE SMEDT, PH., and FRENKEL, D., 1989, *Molec. Phys.*, **68**, 931.
[23] SMIT, B., and FRENKEL, D., 1989, *Molec. Phys.*, **68**, 951.
[24] ALLEN, M. P., and TILDESLEY, D. J., 1987, *Computer Simulation of Liquids* (Clarendon Press).
[25] WOOD, W. W., and PARKER, F. R., 1957, *J. chem. Phys.*, **27**, 720.
[26] WOOD, W. W., 1968, *Physics of Simple Liquids*, edited by H. N. V. TEMPERLEY, J. S. ROWLINSON and G. S. RUSHBROOKE (North-Holland).
[27] ADAMS, D. J., 1979, *Molec. Phys.*, **37**, 211.
[28] NAKANISHI, K., 1986, *Physica*, **139 & 140B**, 148.
[29] SHAW, M. S., 1988, *J. chem. Phys.*, **89**, 2312.
[30] SAAGER, B., and FISCHER, J., 1990, *Fluid Phase Equilibria*, **57**, 35.
[31] VOGELSANG, R., and HOHEISEL, C., 1985, *Molec. Phys.*, **55**, 1339.
[32] THOMPSON, S. M., 1992, unpublished data.
[33] BISHOP, M., and FRINKS, S., 1987, *J. chem. Phys.*, **87**, 3675.
[34] SWOPE, W. C., ANDERSEN, H. C., BERENS, P. H., and WILSON, K. R., 1982, *J. chem. Phys.*, **76**, 637.
[35] CHOKAPPA, D. K., and CLANCY, P., 1988, *Molec. Phys.*, **65**, 97.
[36] BARKER, J. A., and HENDERSON, D., 1967, *J. chem. Phys.*, **47**, 2856, 4714.
[37] WEEKS, J. D., CHANDLER, D., and ANDERSEN, H. C., 1971, *J. chem. Phys.*, **54**, 5237.
[38] CARNAHAN, N. F., and STARLING, K. E., 1969, *J. chem. Phys.*, **51**, 635.
[39] JACOBSEN, R. T., 1972, Ph.D. Thesis, Washington State University; JACOBSEN, R. T., STEWART, R. B., 1973, *J. Phys. Chem. Ref. Data*, **2**, 757.
[40] BARKER, J. A., LEONARD, P. J., and POMPE, A., 1966, *J. chem. Phys.*, **44**, 4206.
[41] GUGGENHEIM, E. A., 1945, *J. chem. Phys.*, **13**, 253.
[42] MORÉ, J. J., GARBOW, B. S., and HILLSTROM, K. E., 1980, *User Guide for Minpack*-1, Argonne National Labs Report ANL-80-74.
[43] SCHMIDT, R., and WAGNER, W., 1985, *Fluid Phase Equilibria*, **19**, 175.
[44] POWLES, J. G., 1984, *Physica A*, **126**, 289.
[45] RICE, S. A., and GRAY, P., 1964, Supplement in FISHER, I. Z., *Statistical Theory of Liquids*, (University of Chicago Press).
[46] REDDY, M. R., and O'SHEA, S. F., 1986, *Can. J. Phys.*, **64**, 677.
[47] MCDONALD, I. R., 1973, *Statistical Mechanics*, Vol. 1, edited by K. Singer (Specialist Periodical Report, The Chemical Society).
[48] SHING, K. S., and GUBBINS, K. E., 1982, *Molec. Phys.*, **46**, 1109; 1983, **49**, 1121.
[49] HARISMIADIS, V. I., KOUTRAS, N. K., TASSIOS, D. P., and PANAGIOTOPOULOS, A. Z., 1991, *Fluid Phase Equilibria*, **65**, 1.